Dual-Atoms Iron Sites Boost the Kinetics of Reversible Conversion of Polysulfide for High-Performance Lithium-Sulfur Batteries

Yue Qiu[‡], Xun Sun[‡], Maoxu Wang[‡], Xian Wu[‡], Bo Jiang[‡], Da Tian[‡], Xueqing Song[‡], Xiaoju Yin[‡], Yu Zhang[‡], Dongyan Tang[‡], Lishuang Fan[*†, ‡], and Naiqing Zhang[*†, ‡]

†State Key Laboratory of Urban Water Resource and Environment, School of Chemistry and Chemical Engineering. Harbin Institute of Technology, Harbin 150001, China.

‡ Academy of Fundamental and Interdisciplinary Sciences, Harbin Institute of Technology, Harbin 150001, China.

*Corresponding Author:

Naiqing Zhang: znqmww@163.com, Lishuang Fan: fanlsh@hit.edu.cn.

Tel: +451 86412153 Fax: +86-451-86412153

Supporting Information:

Part I: Experimental Section

1. material synthesis

1.1. Synthesis of Fe SAs-NC

In a typical procedure, 100 ml Graphene oxide (GO) suspension (1 mg ml^{-1}) was sonicated for 3 h to ensure the homogeneous dispersion. 1 ml $FeCl_3$ $6H_2O$ (4 mg ml^{-1}) aqueous solution was added dropwise into the GO suspension under vigorous sonication and sonicated for another 30 min. The as-obtained precursor powder was collected by rapid freezing in liquid nitrogen and freeze-drying at -70 °C. The dried precursor was then heated at 750 °C under a gas flow of NH_3 and kept for 1 h to obtain Fe SAs-NC.

1.2 Synthesis of Fe DAs-NC

Typically, the as-obtained Fe SAs-NC (100 mg) was dispersed in 100 ml of n-hexane by sonication. Then, 1 mL of $Fe(acac)_2$ ethanol solution was added dropwise into the above suspension under vigorous ultrasound for 30 min, followed by stirring at room temperature for another 2 h. the procedure was centrifuged, washed and dried in vacuum at 60 ℃ overnight. The dried precursor was calcined at 650 °C under a gas flow of NH_3 atmosphere for 2h. The Fe SAs-NC used for comparison was also synthesized by similar method except for adding twice amount of Fe(III) chloride in first step and dropping ethanol solution without $Fe(acac)_2$ in second step.

1.3 Synthesis of Fe DAs-NC/S

The as-prepared Fe DAs-NC were ground with sulfur powder(99.9%, aladdin) in a mass ratio of 2:8 for 30 minutes. Then, the mixture was transferred to a sealed stainless steel

vessel and heated to 155 °C for 12 h to obtain Fe DAs-NC/S. The Fe SAs-NC/S was prepared by the same procedure.

2. Material characterization

The morphology and microstructure images were taken by Hitachi SU8010 scanning electron microscope, Tecnai G2 F30 transmission electron microscopy and JEM-ARM200F spherical aberration corrected scanning transmission electron microscopy (STEM). The crystalline state were characterized by PANalytical X'Pert PRO with Cu-Kα radiation at 40 mA and 40 kV. N_2 adsorption/desorption isotherm and were measured by MICROMERITICS, ASAP 2020 system at 77 K. The corresponding pore size distribution and specific area were calculated by quenched solid density function theory (QSDFT) method and Brunauer-Emmett-Teller (BET) method, respectively. X-ray photoelectron spectroscopy (XPS) was recorded by ThermoFisher ESCALAB 250Xi X-ray photoelectron spectrometer. The Operando X-ray Absorption Spectroscopy Characterization were conducted on the 1W1B beamline at Beijing Synchrotron Radiation Facility (BSRF). The iron content of Fe DAs-NC and Fe SAs-NC were measured by Agilent 5110 ICP-OES.

3. Li-S battery assembling

3.1 Electrode fabrication

The sulfur cathodes were prepared by a general procedure as fallowing: The Fe DAs-NC/S was mixed with Ketchen black (KB) and PVDF in a weight ratio of 80:10:10 and well-milled in N-methyl-2-pyrrolidone (NMP) solvent, then directly coated onto a cleaned aluminum foil by a doctor-balding, the electrode was dried at 60 °C for 12 h and shaped into circular pieces with a diameter of 12 mm with a sulfur loading of about 1.8 mg cm^{-2}. The sulfur-free cathodes were prepared by similar method except for using sulfur-free Fe DAs-NC and Fe SAs-NC materials.

3.2. Cells assembling

3.2.1 Coin cells

Coin cells (CR 2025) for the cycling test were assembled in an argon-filled glove box (<0.1 ppm of H_2O, <0.1 ppm of O_2) with sulfur cathode, lithium metal foil anode and a Celgard 2400 membrane separator. The electrolyte was 25 μL of 1.0 M lithium bis (trifluoromethanesulfonyl)imide (LiTFSI) in 1,3-dioxolane/1,2-dimethoxyethane (DOL/DME) (1:1, v/v) containing 2.0 wt.% of $LiNO_3$. The electrolyte increased to 30 - 40 μL when assembling the lithium sulfur batteries with higher sulfur loading.

3.2.2 Symmetric cells

The Li_2S_6 electrolyte for symmetric batteries containing Li_2S_6 of 0.125 M was prepared by dissolving sulfur and lithium sulfide with stoichiometry into blank electrolyte. The symmetric batteries were assembled in the sequence of sulfur-free electrodes, 20 μL Li_2S_6 electrolyte, Celgard® 2400 membrane, 20 μL Li_2S_6 electrolyte, and the same sulfur-free electrode.

4. Electrochemical measurement

4.1 Symmetric cell characterization

The cyclic voltammetry curves of symmetric cells were scanned at 1 mV s^{-1} between -0.8 V and 0.8 V. The electrochemical impedance spectroscopy was measured in a frequency range from 10^5 to 1 Hz.

4.2 Li_2S nucleation/ dissolution measurement

The Li_2S_8 cells were first assembled by layer in the sequence of sulfur-free electrodes, 20 μL Li_2S_8 electrolyte, Celgard® 2400 membrane, 20 μL blank electrolyte, and metal lithium anode. For Li_2S nucleation measurement, the cells were discharged galvanostatically at 1/24 C to 2.15 V and then discharged potentiostatically at 2.05 V.

For Li_2S dissolution measurement, the Li_2S_8 cells were firstly discharged galvanostatically at 1/24 C to 1.7 V to ensure the full transformation of S to solid Li_2S. Then potentiostatically charged at 2.40 V for the dissolution of Li_2S into LiPS until charge current was below 10^{-5} A. The current and times was simultaneously recorded in whole process to evaluate the nucleation/ dissolution behavers of Li_2S.

4.3 Cyclic voltammetry characterization

The CV characterization of ordinary cells (assembled in 3.2.1) was tested at a scan rate of 0.1 mV/s and voltage window of 1.7 – 2.8 V on ChenHua CHI-760 electrochemical workstation. The Tafel slopes were calculated in initial reduction and initial oxidation process according to the equation: $E=E_0+b \log (j/j_0)$, where E is the electrode potential, E_0 is the equilibrium potential, j is the detected current density, j is the exchange current density and b is the Tafel slope.

4.4 Cycling tests

The charging and discharging performances of the Li-S cells were measured on a NEWARE BTS TC53 analyzer under a potential window of 1.7-2.8 V vs. Li^+/Li. Before all the cycling tests, the cells were activated by charged and discharged at 0.1 C (1 C=1672 mAh g^{-1}) for 3 cycles. Rate performance were measured under 0.2, 0.5, 0.1, 2.0, 5.0 by 5 cycles in each C, the long cycling test was conducted at 0.5 C for 400 cycles and 2 C for 2000 cycles, and the high loading cells were cycled at 0.2 C for 200 cycles.

5. Visible adsorption observation

The adsorption capacity of different materials for polysulfide was evaluated by contrasting the color change of the solution after a certain period of time when materials with the same surface area were added to the polysulfide solution. Here, 20 mg of Fe DAs-NC and Fe SAs-NC are added in 3.0 mL Li_2S_4 solution with a concentration of 20

mM [S]. The digital photo of the solutions was taken by the camera of MI 10 PRO 5G after standing for 12.0 h. Corresponding UV/vis spectra were also acquired to further compare the adsorption capacity.

6. Computation Methods and Models

We have employed the Vienna Ab Initio Package (VASP)[1,2] to perform all the spin-polarized density functional theory (DFT) calculations within the generalized gradient approximation (GGA) using the PBE[3] formulation. We have chosen the projected augmented wave (PAW) potentials[4,5] to describe the ionic cores and take valence electrons into account using a plane wave basis set with a kinetic energy cutoff of 400 eV. Partial occupancies of the Kohn−Sham orbitals were allowed using the Gaussian smearing method and a width of 0.05 eV. The electronic energy was considered self-consistent when the energy change was smaller than 10^{-7} eV. The DFT-D3 empirical correction method was employed to describe van der Waals interactions.

The adsorption energy (E_{ads}) of adsorbate A was defined as:

$$E_{ads} = E_{A/S} - E_S - E_{A(g)}$$

where $E_{A/S}$, E_s and $E_{A(g)}$ are the energy of adsorbate A adsorbed on the graphene monolayer, the energy of clean graphene monolayer, and the energy of isolated A molecule in a cubic periodic box with a side length of 20 Å and a 1×1×1 Monkhorst-Pack k-point grid for Brillouin zone sampling, respectively.

Part II: Supplementary Results

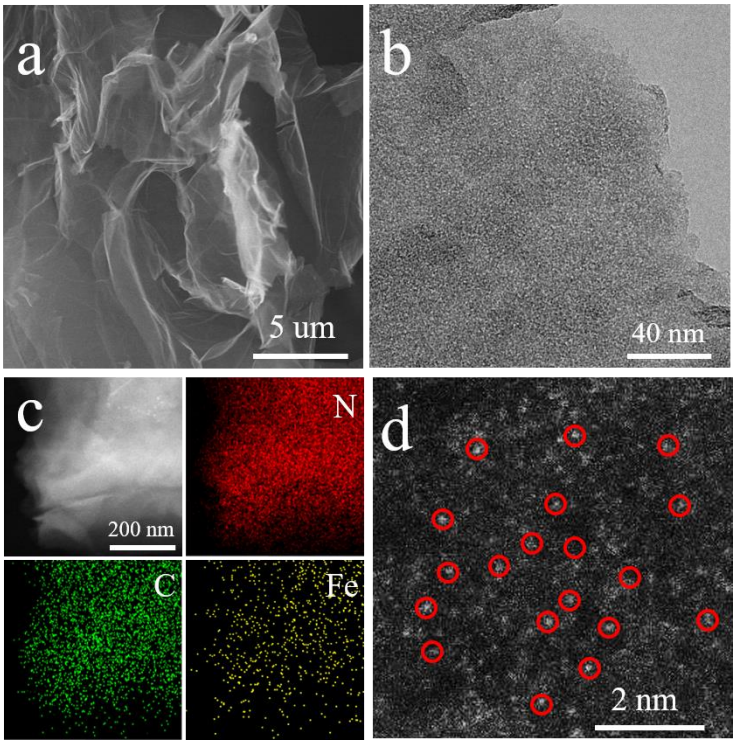

Figure S 1 (a) SEM and (b) HRTEM images and (d) partial magnified images of Fe SAs-NC, and corresponding EDS elemental mapping profiles of Fe, N and C. (c) Aberration-corrected HAADF-STEM.

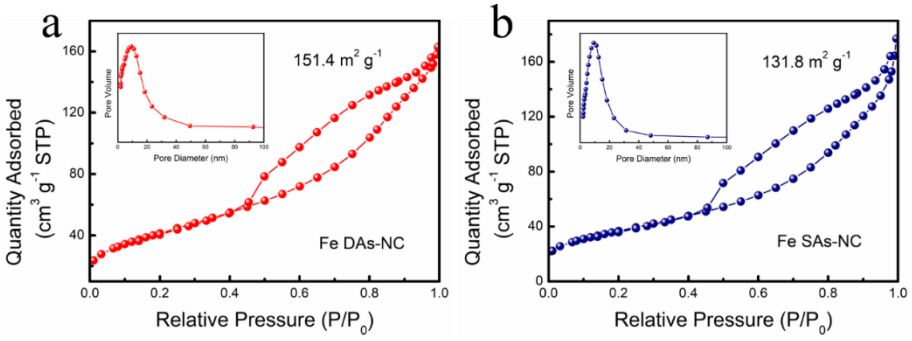

Figure S 2 N_2 adsorption/desorption isotherm (inset: pore size distribution) of as-synthesized (a) Fe DAs-NC and (b) Fe SAs-NC.

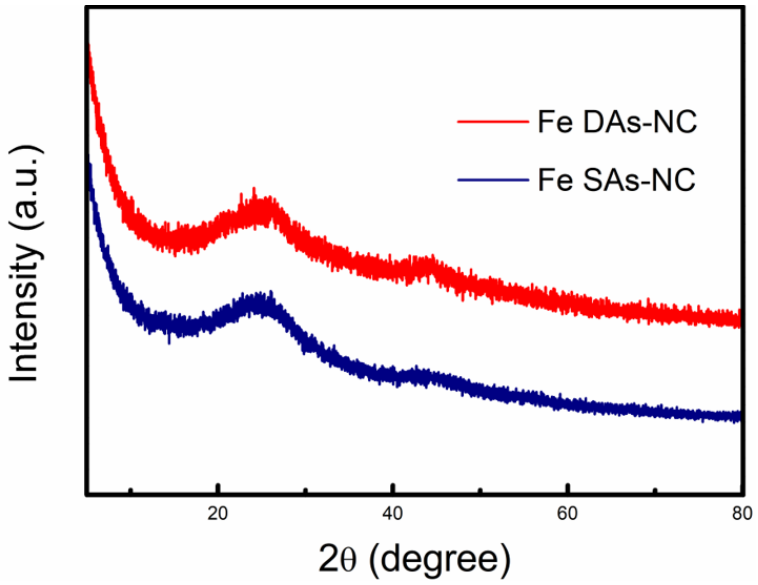

Figure S 3 XRD patterns of Fe DAs-NC and Fe SAs-NC.

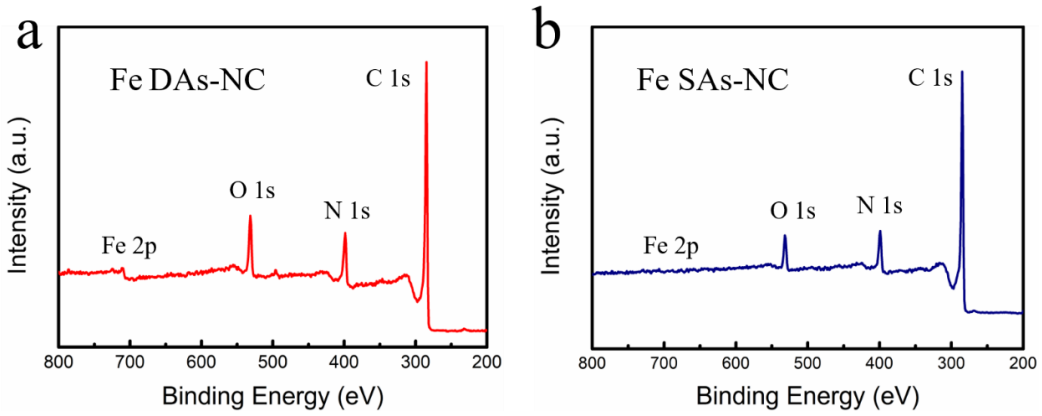

Figure S 4 XPS survey spectra of (a) Fe DAs-NC and (b) Fe SAs-NC. The higher O content of Fe DAs-NC is due to its stronger adsorption capacity for oxygen in the air.

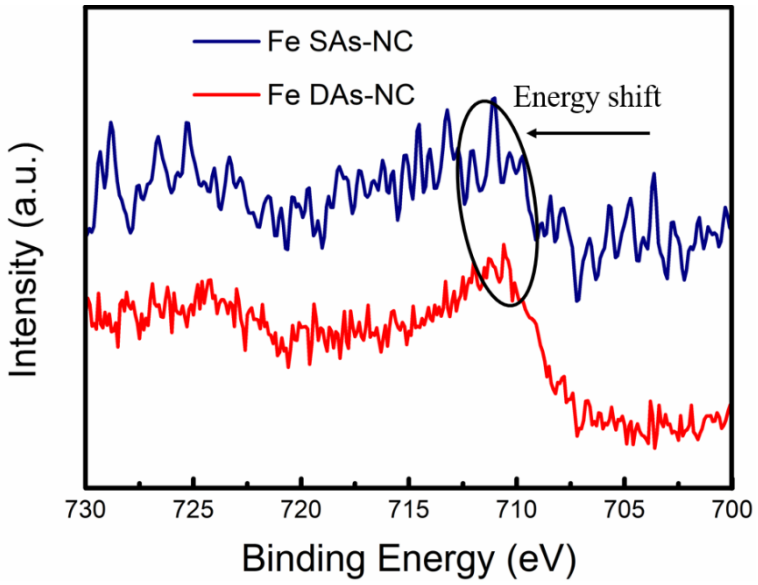

Figure S 5 Fe 2p XPS spectra of Fe DAs-NC and Fe SAs-NC. The negative energy shift of Fe DAs-NC compared with that of Fe SAs-NC, suggesting its lower oxide degree of Fe.

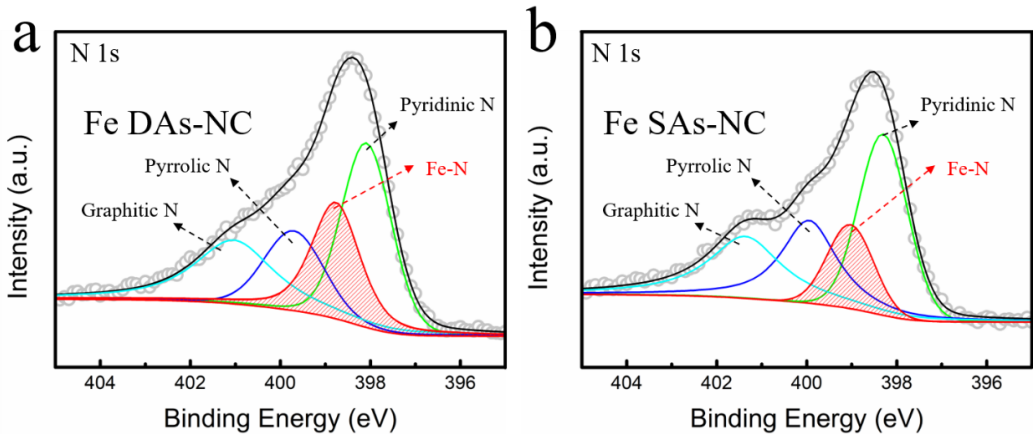

Figure S 6 High-resolution N 1s XPS spectra of the (a) Fe DAs-NC and (b) Fe SAs-NC.

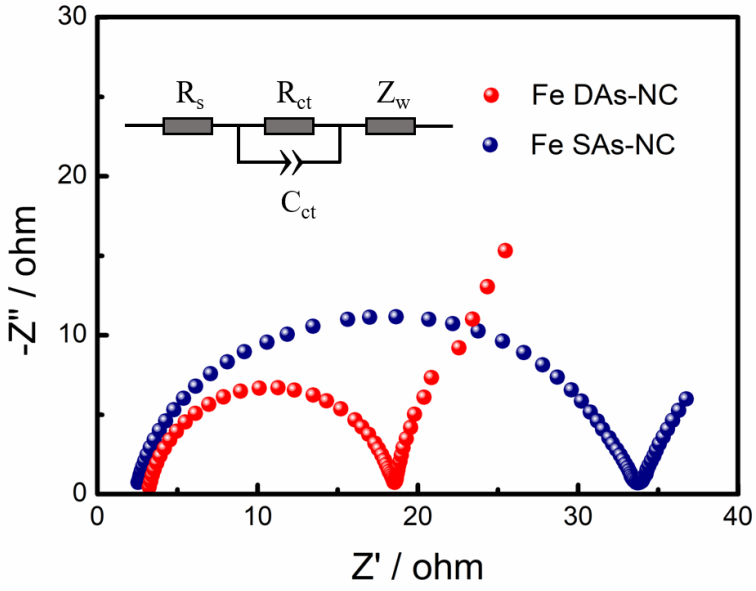

Figure S 7 Nyquist plots and corresponding fitting circuit diagram of symmetric cell with Fe DAs-NC and Fe SAs-NC electrode

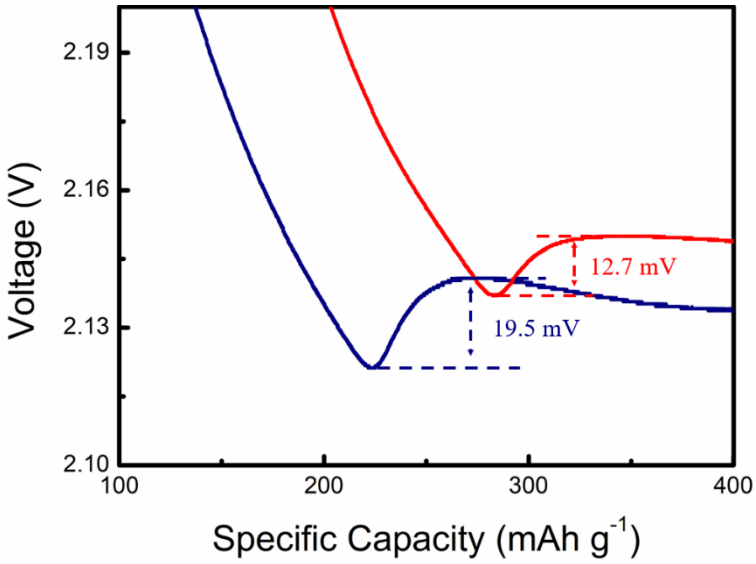

Figure S 8 Galvanostatic discharge profiles of Li|Li_2S_8 cells with Fe DAs-NC and Fe SAs-NC cathodes at C/24.

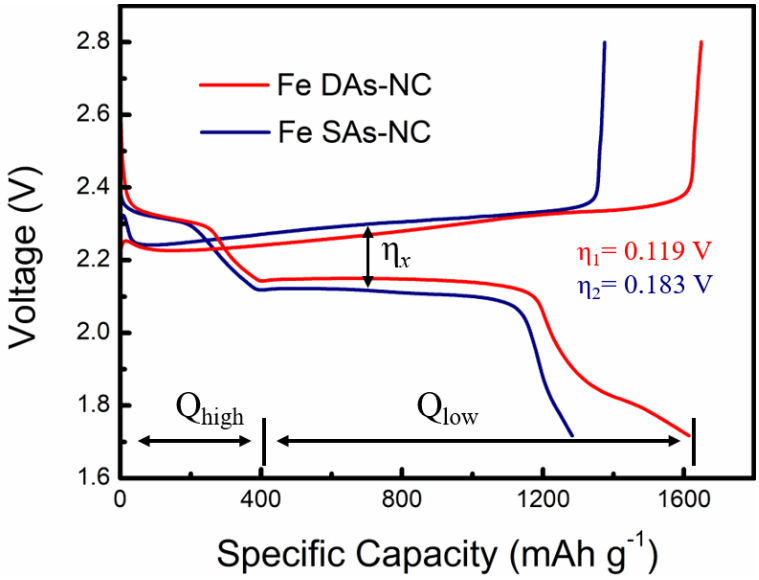

Figure S 9 Galvanostatic charge/discharge profiles of Li-S batteries based on Fe DAs-NC/S and Fe SAs-NC/S cathodes at 0.05 C.

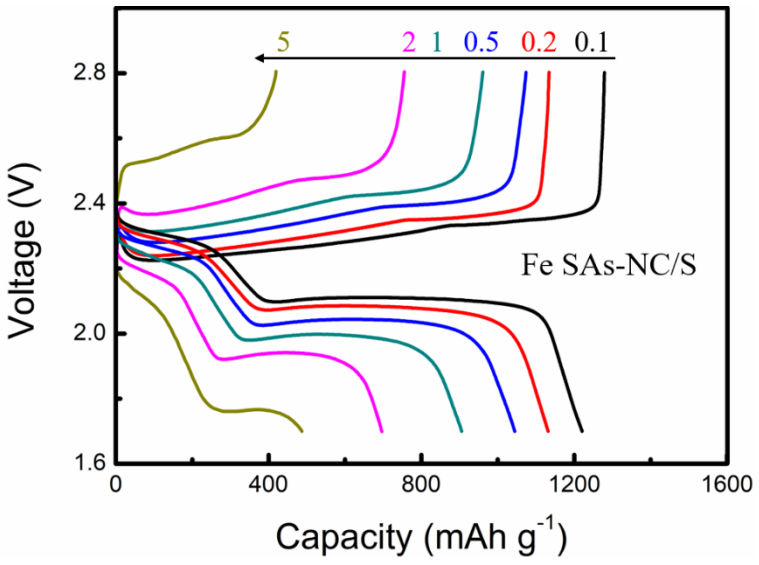

Figure S 10 galvanostatic charge-discharge curves of Li-S battery based on Fe SAs-NC/S cathodes at 0.1, 0.2, 0.5, 1, 2 and 5 C.

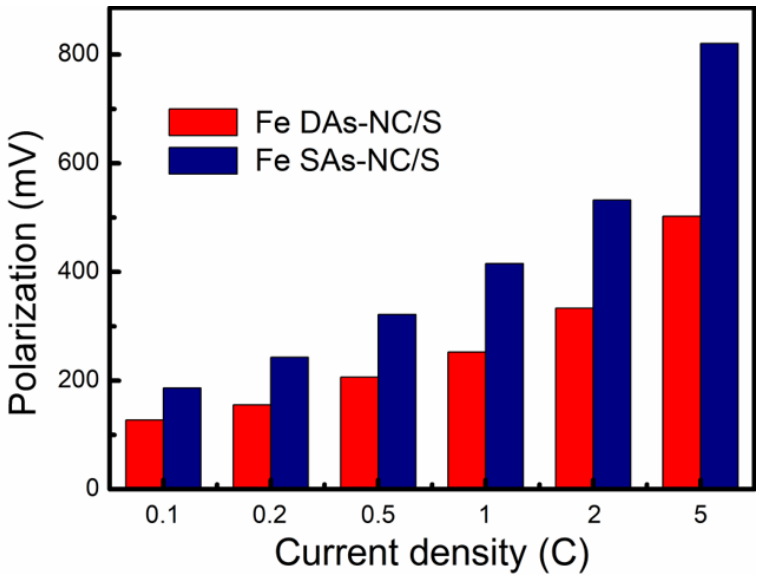

Figure S 11 overpotential of batteries based on Fe DAs-NC/S and Fe SAs-NC/S cathodes at different current density.

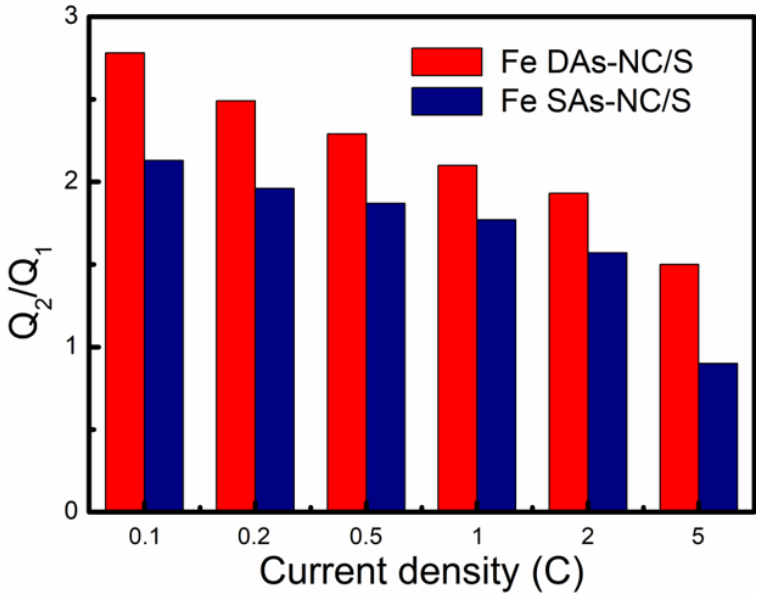

Figure S 12 The ratios(Q_2/Q_1) of two discharge plateau(Q_1 for the first plateau and Q_2 for the second plateau) at various current rates for Li-S batteries based on Fe DAs-NC/S and Fe SAs-NC/S cathodes.

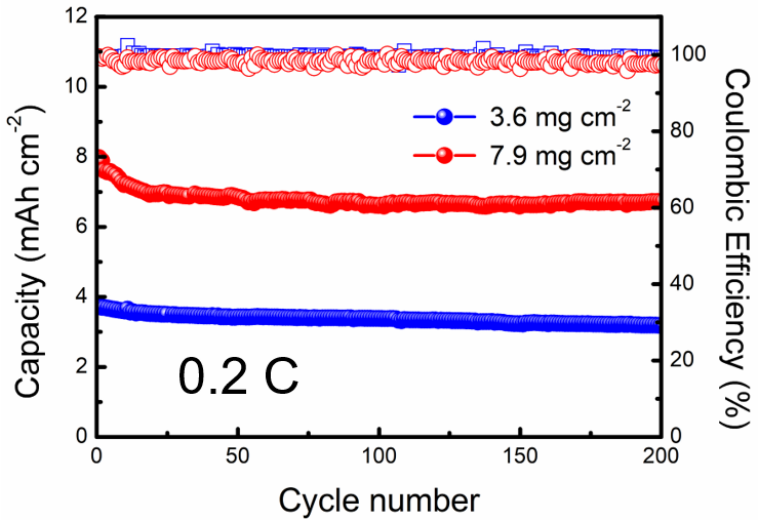

Figure S 13 Cycle performance of batteries with Fe DAs-NC/S cathodes in high sulfur loading at 0.2 C.

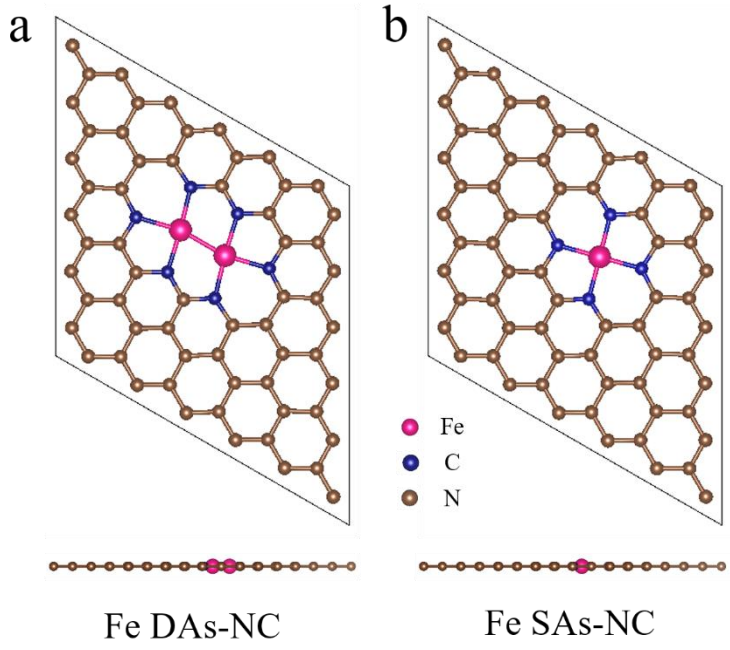

Figure S 14 The optimized coordination structure models of (a) Fe DAs-NC and (b) Fe SAs-NC according to the XAS and XPS results.

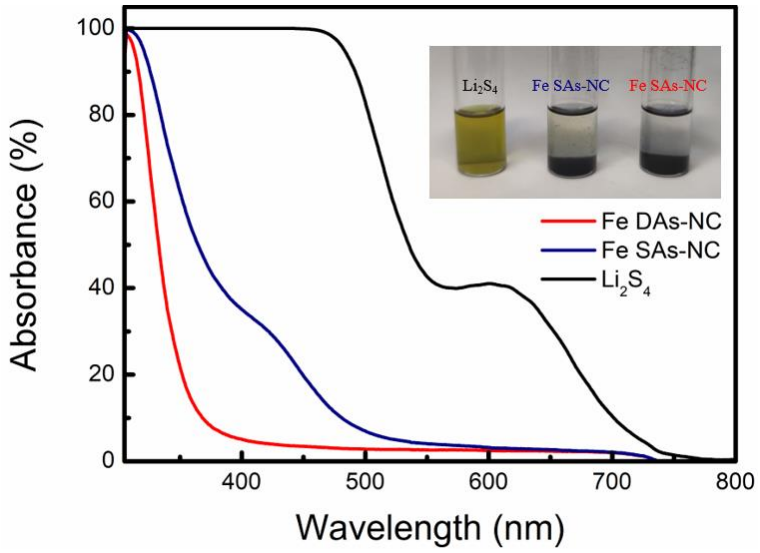

Figure S 15 Optical photograph of bare Li_2S_4 solution and Li_2S_4 solution with Fe DAs-NC and Fe SAs-NC (inside), and corresponding UV-vis spectra of above solution after aged for 12 h.

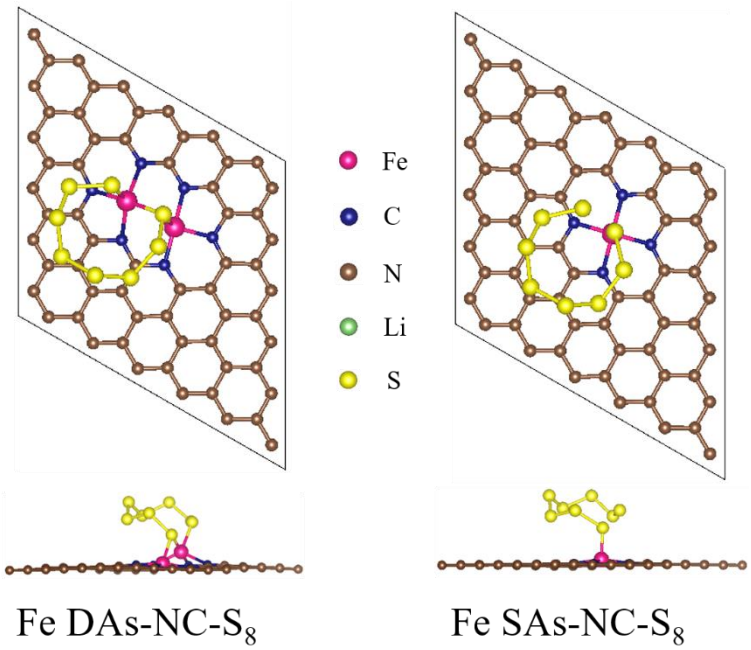

Figure S 16 Optimized configurations of S_8 anchored on (a) dual-atoms Fe site and (b) single atom Fe site.

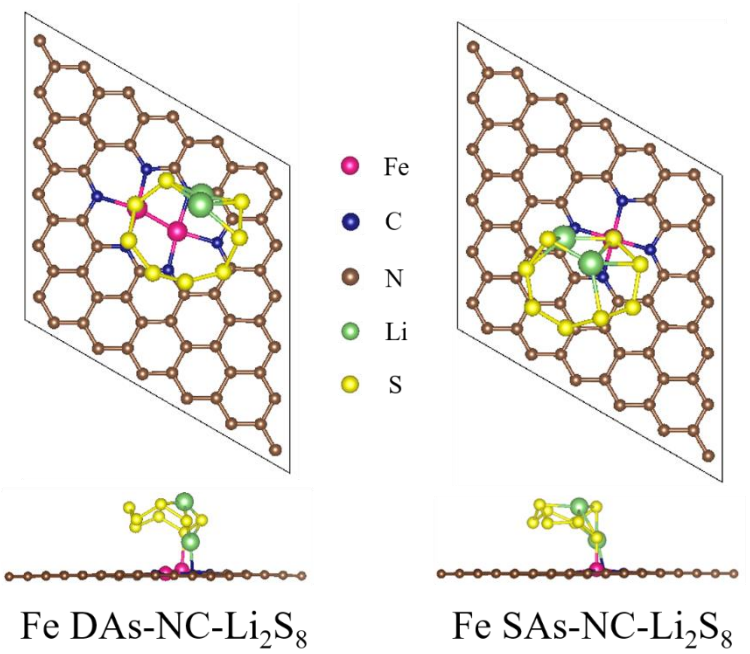

Figure S 17 Optimized configurations of Li_2S_8 anchored on (a) dual-atoms Fe site and (b) single atom Fe site

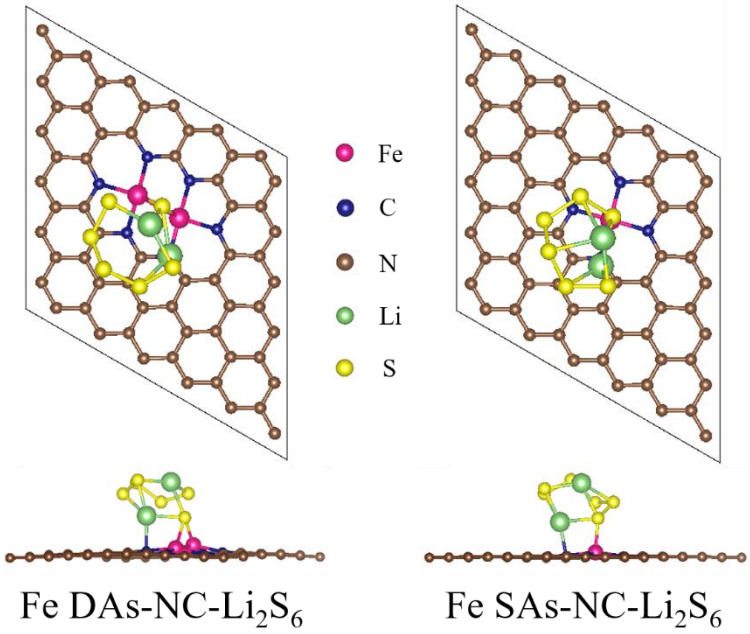

Figure S 18 Optimized configurations of Li_2S_6 anchored on (a) dual-atoms Fe site and (b) single atom Fe site

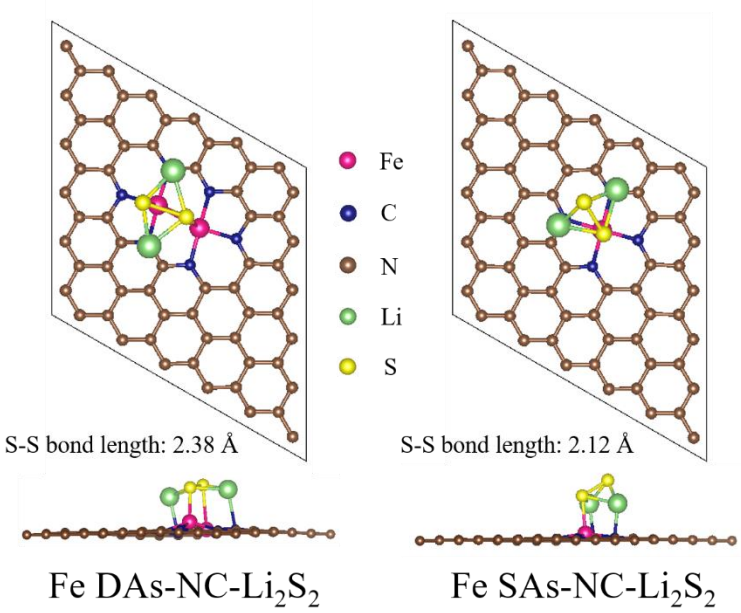

Figure S 19 Optimized configurations of Li_2S_2 anchored on (a) dual-atoms Fe site and (b) single atom Fe site with corresponding S-S bond length

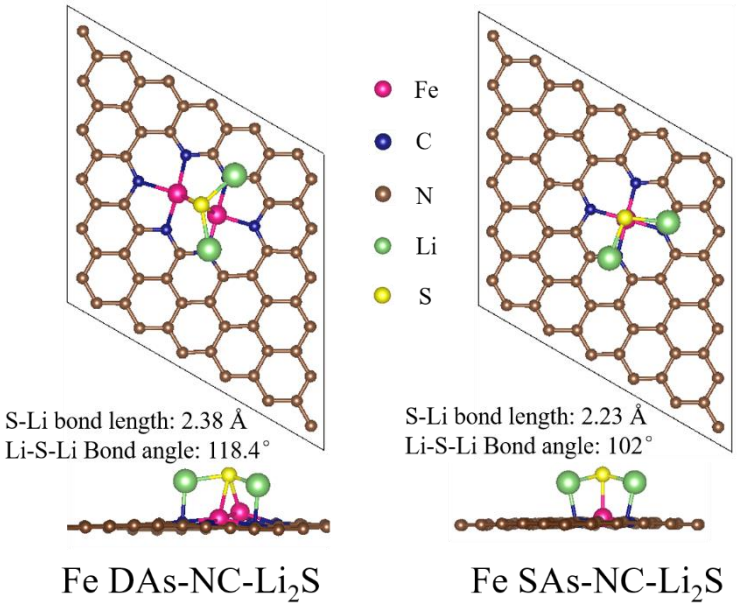

Figure S 20 Optimized configurations of Li_2S anchored on (a) dual-atoms Fe site and (b) single atom Fe site with corresponding S-Li bond length and Li-S-Li bond angle

Table S 2 Fe K-edge EXAFS fitting parameters of various samples（$S_0^2 = 0.84$）

sample	Path	C.N.	ΔE(eV)	100xR(Å)	$10^3 x\sigma^2$(Å²)	R-factor
Fe foil	Fe-Fe1	8	3.054(1.86)	245.6(1.3)	5.85(1.58)	0.007
	Fe-Fe2	6	3.054(1.86)	283.2(1.1)	4.94(1.95)	
	Fe-Fe3	12	3.054(1.86)	404.3(2.3)	9.47(2.43)	
Fe_2O_3	Fe-O	6	7.56(3.32)	196.3(2.4)	11.95(2.13)	0.004
	Fe-Fe	6	1.96(0.38)	299.1(1.8)	9.85(1.52)	
Fe DAs-NC	Fe-N	3.4	5.88(1.37)	202.5(3.3)	2.92(0.92)	0.003
	Fe-Fe	1.1	8.84(3.13)	233.9(2.3)	12.35(3.14)	
Fe SAs-NC	Fe-N	4.2	1.85(0.32)	202.8(0.6)	8.69(0.94)	0.001

C.N.: coordination numbers; *R*: bond distance; σ^2: Debye-Waller factors; ΔE_0: the inner potential correction. *R* factor: goodness of fit. * the experimental EXAFS fit of metal foil by fixing CN as the known crystallographic value.

References

1. Kresse, G.; Furthmüller, J. Efficiency of Ab-Initio Total Energy Calculations for Metals and Semiconductors Using a Plane-Wave Basis Set. Comput. Mater. Sci. 1996, 6, 15−50.
2. Kresse, G.; Furthmüller, J. Efficient Iterative Schemes for Ab Initio Total-Energy Calculations Using a Plane-Wave Basis Set. Phys. Rev. B 1996, 54, 11169−11186.
3. Perdew, J. P.; Burke, K.; Ernzerhof, M. Generalized Gradient Approximation Made Simple. Phys. Rev. Lett. 1996, 77, 3865−3868.
4. Kresse, G.; Joubert, D. From Ultrasoft Pseudopotentials to the Projector Augmented-Wave Method. Phys. Rev. B 1999, 59, 1758-1775.
5. Blöchl, P. E. Projector Augmented-Wave Method. Phys. Rev. B 1994, 50, 17953−17979.